Eur. Phys. J. D **29**, 33–38 (2004)
DOI: 10.1140/epjd/e2004-00007-5

THE EUROPEAN PHYSICAL JOURNAL D

Atomic scale models of Co−Ag mixed nanoclusters at thermodynamic equilibrium

T. Van Hoof and M. Hou[a]

Physique des Solides Irradiés et des Nanostructures, CP 234, Université Libre de Bruxelles, boulevard du Triomphe, 1050 Brussels, Belgium

Received 1st October 2003
Published online 27 January 2004 –

Abstract. The configurations at thermodynamic equilibrium of Co_xAg_{201-x} nanoparticles are explored for $0 < x < 201$ by means of Metropolis Monte Carlo simulations with a semi-empirical embedded atom potential at temperatures from 100 K to 1000 K. Remarkable configurations are predicted in this temperature range. As a consequence of a competition between strain and Co binding at low temperature, for $x < 20$, Co is distributed just below the cluster surface layer into groups of no more than 5 atoms, favouring well-defined positions, and the cluster central area is avoided. To increase the temperature favours the clustering of these small groups. Their dissolution is predicted at temperatures higher than the melting temperature of the cluster. For $x > 50$, Co regroups at the centre of the cluster and intersects {111}-facets when Ag atoms are not numerous enough to form an entire surface shell. At these stoechiometries, temperature is not sufficient to mix Ag and Co, even above the melting point. At still smaller Ag concentrations, the Ag atoms are distributed at lowest coordination sites, along the edges of the cluster, avoiding the cluster facets as well as inner sites. At intermediate stoechiometries ($20 < x < 50$), either oblate Co groups below the surface or a compact group at the centre of the cluster are possible.

PACS. 61.46.+w Nanoscale materials: clusters, nanoparticles, nanotubes, and nanocrystals – 61.43.Bn Structural modeling: serial-addition models, computer simulation

1 Introduction

Bimetallic nanoparticles attract much interest for their specific catalytic, optical or magnetic properties. The possibility to tune their stoechiometry when forming solid solutions allows to modifying their properties in a controlled way. An important issue to catalytic and optical properties is the possible cluster composition difference between the surface and the core. Quantitative experimental determination of the cluster surface composition is difficult and it often requires the support of atomic scale modelling. Modelling methods have been developed to this purpose or adapted from methods designed for bulk materials [1–5]. They are grounded on semi-empirical cohesion models which parameters are generally adjusted to reproduce known alloy properties. However, not only miscible, but also non-miscible systems are promoting significant interest. The deposition of monokinetic Co atoms on a Ag surface in the soft landing regime showed ballistic effects in Co island nucleation and growth [6,7]. Co nanoclusters deposited on silver were found burrowing partially [8] and, when entirely buried, strong size dependent interfacial strain was found [9]. Phase separation induced Co_xAg_{1-x} granular thin films was studied as well [10–12]. This illustrates the possibility of forming materials with non-miscible elements. Their nanostructure can be different from the nanostructure of miscible systems. Electrical properties and, more frequently, magnetic properties of systems formed by buried Co clusters in Ag were subjected to experimental, modelling and theoretical studies. Percolation conditions were found [13], the Co cluster size dependence of magnetic properties was evidenced [14,15], the temperature dependence of magnetisation was measured [16] as well as the correlation between magnetic and optical properties [17]. In these studies, either pure Co clusters are in contact with a pure Ag matrix, or granular films are formed which composition and structure are governed by mechanical and thermodynamic conditions. However, the possibility to produce mixed non-miscible bi-metallic clusters way out of thermodynamic conditions with any composition [18,19] should presently allow tuning the stoichiometry and structure of granular films in a controlled way. Clusters formed by cobalt and silver atoms represent one such example. It is the purpose of the present work to correlate the stoechiometry of non miscible clusters with atomic configurations at thermodynamic equilibrium, and the interplay between binding energy, surface strain and temperature will be emphasised. Section 2 summarises the features of the atomic scale method

[a] e-mail: mhou@ulb.ac.be

used. The results are described and discussed in Section 3 and a synthesis is given in Section 4.

2 The simulation method

It is the purpose of the present work to provide configuration models for small Co_xAg_{n-x} clusters, whose properties specific to the non-miscible nature of the cobalt-silver system will be emphasised. Here, we choose $n = 201$. This is the smallest number of atoms with which it is possible to build an ideal truncated octahedron with the fcc structure [20]. It is formed by 8 {111}-facets and 6 {100}-facets. There are 24 vortices, 60 atoms form the edges and the whole surface contains 122 atomic sites. It is desired, for a given x, to find the thermodynamic equilibrium configuration of the cluster at a given temperature. This requires to find the configuration minimising the Helmholtz free energy of the system. The evolution of a cluster to equilibrium may be very slow. Molecular Dynamics (MD) was already used to study cluster alloying [4,5]. In these studies, the equations of motion were integrated over a time of the order of the microsecond, which nowadays represent the longest practically possible integration time. The speed at which alloying takes place depends on the available kinetic pathways, themselves depending on the defect state of the system. Model compact nanoclusters may not display such defects. A convenient method, which may avoid following a kinetic pathway, is the Metropolis Monte Carlo (MMC) importance sampling method. The method was successfully employed in [3,21] where the sampling was achieved in the so-called semi-grand canonical ensemble [22]. In this ensemble, the total number of particles, the pressure and the temperature are fixed, as well as the chemical potential difference between two species forming the system. This method, suitable for alloy phases and solid solutions, is simpler in the case of non-miscible systems. For these, the sampling is achieved in the canonical (NPT) ensemble. In this ensemble, not only the total number of particles is constant but also the number of particles of each species. Since, in the present case, the surface of the cluster is free, the external pressure is zero. The sampling scheme includes two types of trials. (i) Random displacement of each atom in the cluster from each current position. (ii) Random site exchange between two chemically different atoms. Optionally, trials on the global volume change are performed as well. A trial is accepted if it lowers the configuration energy of the system. Trials (i) and (ii) are accepted as well with a probability

$$P = e^{-\Delta U/kT} \tag{1}$$

if the configuration energy increased. ΔU is the configuration energy difference. Global volume changes are accepted with a probability

$$P = e^{-[\Delta U - Nk\log(V_N/V_0)]/kT} \tag{2}$$

where V_N and V_0 are the attempted and the current volume of the system respectively. The magnitude of the moves in (i) is dynamically adjusted in order to maintain a rate of acceptance close to 0.4, which is empirically found to optimise convergence. Trials (ii) correspond to no physical evolution path for the system. The advantage of using exchange trials is to limit the risk of trapping the system into a local minimum because of high energy barriers. The configuration energy difference ΔU appears to be the determinant factor in the free energy minimisation. Semi-empirical methods are currently used to evaluate configuration energies.

In the embedded atom method (EAM) [23], the expression of the cohesive energy is given by

$$E_i = \frac{1}{2}\sum_{j\neq i} V_{\alpha\beta}(r_{ij}) - F_\alpha(\rho_i) \tag{3}$$

where the electronic density ρ_i at site i is given as

$$\rho_i = \sum_j \varphi_j(r_{ij}). \tag{4}$$

As it appears in (3), the N-body term is given by a function F_α of the local electronic density ρ_i due to atoms neighbouring atom i. F_α depends of the chemical nature of the embedded atom i and is often obtained by fitting the model to the universal equation of state of Rose [24]. In this model, only the parameters of the mixed repulsive part $V_{\alpha\beta}$ need to be adjusted to binary systems properties. A further simplification, proposed by Johnson, is to express the mixed repulsive part as a weighted average of the pure repulsive components $V_{\alpha\alpha}$ and $V_{\beta\beta}$ [25]. This approximation has no strong physical grounds but it was successfully used to calculate heat of solutions in binary alloys made of Au, Cu, Ag, Ni, Pd and Pt [25,26]. A single parameter can however be introduced to fit the mixed repulsive part in order to predict physical properties better accurately. In the case of non-miscible systems, the number of available experimental data to adjust the parameters is generally limited or non existent. When they are lacking, it is possible to refer to ab initio calculations as done, for instance, in [27,28]. For the Co–Ag system however, a range of experimental data is available allowing the assessment of a semi-empirical parameterisation.

Regarding the uncertainty about the strength of mixed repulsive potential term in (3), we scale this component with one adjustable parameter for fitting to available experiment. The only experimental data used for this fitting data [9] is the interatomic distance in a Co dimer embedded in a silver matrix at 77 K, as measured by EXAFS [29]. The strength of the mixed part of the Co–Ag potential turned out to be the best estimated with the weighted average in [25] with a scaling parameter equal to one. Using this value, the potential was assessed by comparing the predicted and measured Co–Ag distances at the interface of a Co cluster in Ag at low temperature. The Debye temperature Θ_D of substitutional Co and of the Co dimer was evaluated by MD and compared with Mössbauer spectroscopy results [9]. The agreement was within the experimental uncertainty. Good agreement was found as well for the size dependence of the Debye temperature of a Co cluster embedded in Ag. We now use

the same potential to examine possible Co_xAg_{201-x} free clusters configurations for $0 < x < 201$. Semi-empirical potentials, like the present EAM potential, generally underestimate surface excess energies. In bi-metallic clusters, this may be a point of concern as size effects are concerned. However, as it comes out of [1] that, although surface energies are too low, predicted surface energy differences are more reasonable. This cannot be checked directly in the present case since the Co structure in the bulk phase and in nanoclusters are different and surface energies are not comparable. The effect of the offset in surface energies on model predictions was carefully studied in [30] for Cu_3Au bulk and nanosize crystals by introducing a coordination dependent correction to the potential. The results confirmed the conclusion reached in [1] for other bi-metallic systems. As segregation is concerned, in the case of Ni–Al alloys, it is not found significantly different at the surface of free clusters and at the interfaces of cluster assemblies where surface areas are reduced [31].

Calculations are performed with the (NPT) Metropolis Monte Carlo algorithm. Each configuration discussed has been obtained by repeating the MMC free energy minimisation using different random number generator seeds, with and without sampling global volume changes, as well as using several initial configurations differing from each other as much as possible. In each case, 5 millions Monte Carlo steps were used. With these precautions, in most cases, it was possible to ensure that the predicted configurations do not depend on the initial conditions. This way, the risk of trapping the system into a local minimum is limited. The simulations were repeated at different temperatures from 100 K to 1000 K, in order to estimate possible thermal effects on cluster configurations in the solid state as well as the effect of the cluster melting.

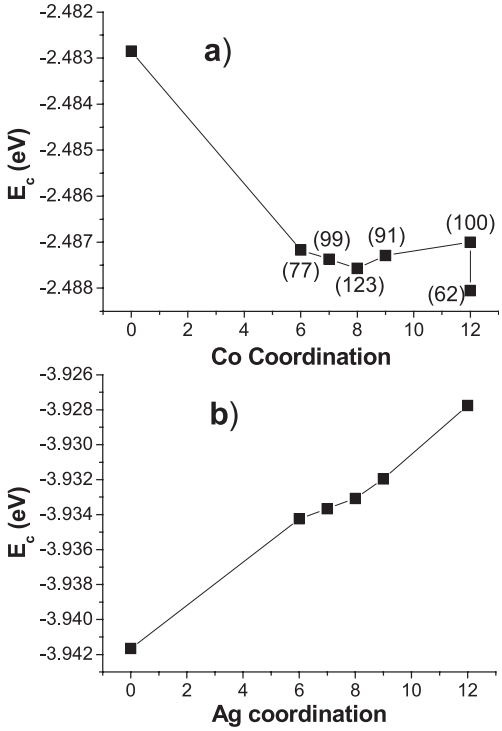

Fig. 1. Configuration energies predicted by molecular statics simulations for (a) $CoAg_{200}$ and (b) $Co_{200}Ag$ truncated octahedral clusters as a function of the coordination of the single atom. 0-coordination represents, for convenience, the configuration energy of the elemental clusters. Coordination 6 corresponds to a vertex, 7 to an edge, 8 to a {100}-facet, 9 to a {111}-facet, 12 to an inner position. In (a), the mean induced Ag displacement is given in (pm). The two points with coordination 12 correspond to the Co atom at the cluster centre (higher energy) and beneath a vertex (lower energy).

3 Results and discussion

This section is subdivided into three parts. We first consider clusters dominantly formed by silver, then clusters dominantly formed by cobalt and finally those with intermediate stoechiometry.

3.1 Co_xAg_{201-x} with $x < 20$

In the whole temperature range where the cluster is solid, a single Co atom buried anywhere in a Ag_{200} cluster has a well-defined equilibrium location as a first neighbour of a vertex, below the cluster surface. Similar configurations were found by molecular dynamics for Cu instead of Co [5]. This indicates the generality of the rule and, in particular, that this configuration is not related to miscibility. The minimal free energy configuration appears as a compromise between two trends. On the one hand, the configuration energy lowers with increasing Co coordination but on the other, it is increased by the Ag relaxation around the Co atom. Thanks to the various different site types in a truncated octahedral cluster, it is possible to estimate the 0 K configuration energy of the cluster as a function of the Co first neighbour coordination. This is done by molecular statics and the results are shown in Figure 1a. Coordination 6 corresponds to a Co position at a vertex, 7 in an edge, 8 in a {100}-facet, 9 in a {111}-facet and 12 inside the cluster. In the figure, the distinction is made between a Co in the centre of the cluster and inside, first neighbouring a vertex. For each configuration, the mean induced displacement of the Ag atoms is given, as relative to the positions in a pure Ag cluster. It clearly comes out that the configuration predicted by Monte Carlo corresponds to the best stable 0 K Co configuration, which also minimises the Ag configurational relaxation. In this configuration, Co is fully coordinated. The same rule is found to apply in other circumstances such as in the case of low index surfaces of bulk silver. The minimal energy equilibrium position of a Co atom is predicted substitutional in the second atomic plane from the surface, the cost of relaxing Ag surface atoms being less than relaxing Ag atoms in the bulk. Similar conclusions were reached with other systems like Co–Cu [27,32].

For $1 < x \leq 20$, the atomic arrangement in the cluster depends on temperature and it is characterised by a balance between the lowering of the energy by clustering

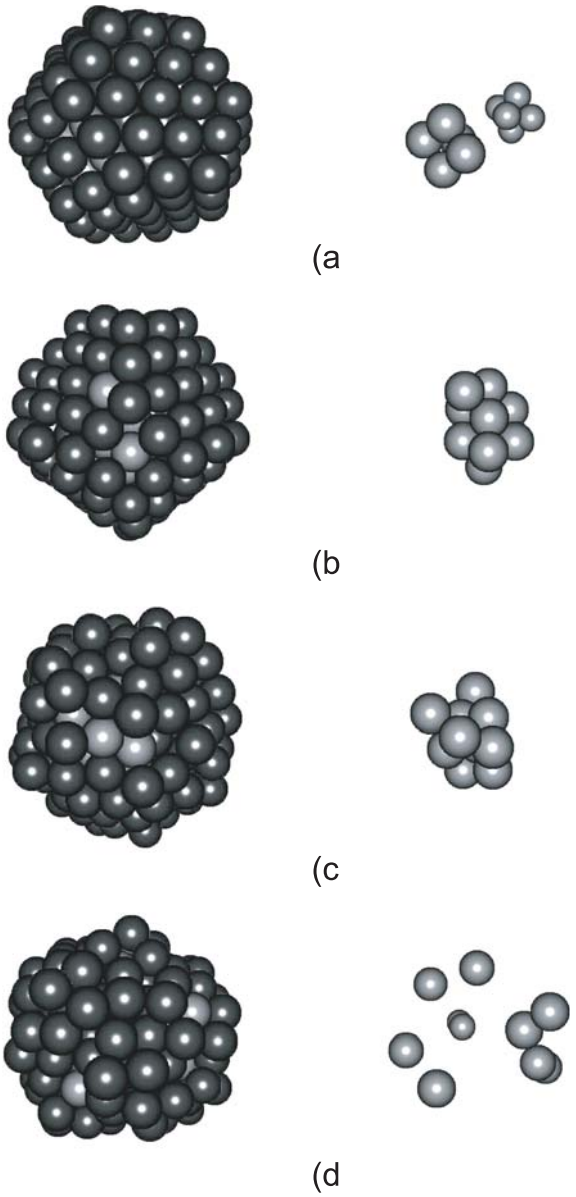

Fig. 2. Several configurations for the $Co_{10}Ag_{191}$ cluster at different temperature. Ag atoms are represented in dark, Co atoms in light. (a) 100 K , (b) 500 K, (c) 700 K and (d) 1000 K. The pictures at the right represent the cobalt atoms only.

of Co atoms and the increase of energy by Ag relaxation. At 100 K, most Co atoms sit below the {100}-facets, first neighbouring a vertex. This can be understood regarding the lower coordination in {100}-facets as compared to {111}-facets and thus the lower energy required to displace the Ag surface atoms. In the temperature range between 100 and 500 K, Co agglomerates forming groups whose sizes increase with temperature. They are generally located just below the {100}-surfaces. Figure2a shows a configuration at 100 K where 10 Co atoms cluster into two groups beneath two opposite {100}-facets. Pyramidal configurations, optimising the Co–Co binding are favoured and the groups contain 5 atoms each. At 500 K and higher, Co atoms are forming one single group (Fig. 2b). The melting temperature of the $Co_{10}A_{201-10}$ cluster was obtained by determining the caloric curve by means of MMC. A clear step was found at 650 K. From this temperature up, the truncated octahedral structure is lost (Fig. 2c). To increase the temperature to 1000 K leads to the dissolution of the Co groups, but the Co remains beneath the cluster surface (Fig. 2d). In bulk silver, such small Co groups are found unstable as well.

In some configurations, Co atoms appear at the surface but the number of Co at the surface is rarely found above 2 percent of the total Co amount. The centre of the cluster appears as a forbidden zone for cobalt. When the Co atoms are artificially regrouped at the centre, their binding energy is not sufficient to balance the excess energy stored in the relaxed Ag system, whatever the temperature.

3.2 Co_xAg_{201-x} with $x > 50$

For these stoechiometries, configurations are not found as highly dependent on temperature. As already found experimentally [13] and predicted by atomic scale modelling [8,9] the fcc structure of a small buried or isolated pure Co cluster is predicted stable. This is confirmed here for Co_{201} isolated clusters in the whole temperature range where it is solid. When one Co atom is replaced by silver, the Ag atom gets to the surface, at a vertex or at an edge. These are minimal coordination Ag configurations found to represent the lowest possible increase of the Co configuration energy. As seen in Figure 1b, the EAM model used predicts only little energy difference between the vertex and the edge configurations. At 0 K, the vertex configuration energy is the lowest. The energy difference with an edge site configuration is less than 1 meV. For this reason, it was not possible to identify the lowest energy one at non-zero temperature. When the amount of silver is increased, it tends to fill the vortices and edges before occupying facets sites. This is illustrated in Figure 3a where 50 Ag atoms share surface sites. In this range of stoechiometry, the Co is regrouped in a compact cluster and Ag atoms tend to cover the whole surface. Since 122 atoms form the surface of the ideal 201 atoms truncated octahedron, when $x > 79$, Co atoms of the central group are necessarily present at the surface. As shown in Figure 3b, they preferentially take part in {111}-facets in which the coordination is higher than in {100}-facets. In Figure 1a, it was found that the configuration energy with one Co in a {100}-facet is lower than if located in a {111}-facet. In the present case however, the effect of a higher Co binding with a higher Co–Co coordination dominates.

3.3 Co_xAg_{201-x} with $20 < x < 50$

These intermediate situations are more complex. The Metropolis algorithm hardly converges as these stoechiometries are at the fringing field where surface trapping and cobalt binding balance each other. Configurations are found where Co either regroup at the centre or

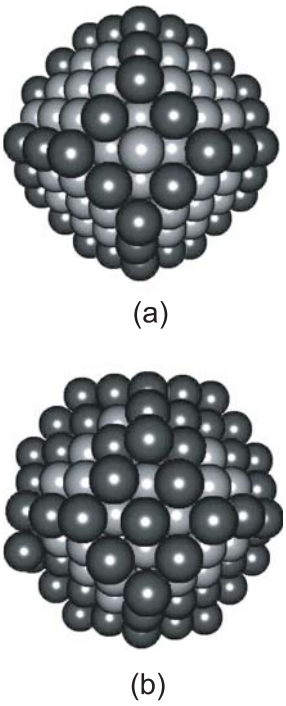

Fig. 3. Calculated configurations of $C_{151}Ag_{50}$ (a) and $Co_{101}Ag_{100}$ (b) clusters. Ag atoms are represented in dark, Co atoms in light.

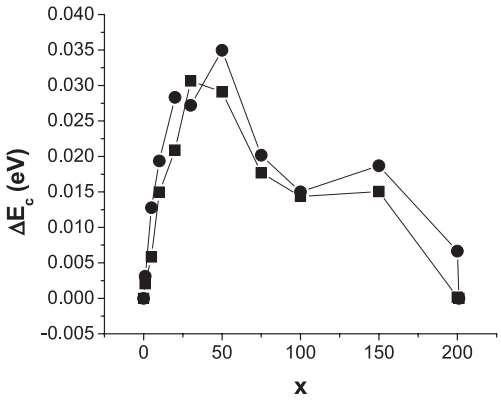

Fig. 4. Excess energies of Co_xAg_{201-x} clusters as a function of x. Results are shown after quenching for the cluster configurations predicted by Metropolis Monte Carlo (squares) and for configurations where Co groups of atoms occupy first neighbour lattice sites isotropically distributed around the centre of the cluster (circles).

form oblate groups below the surface, avoiding the central area. Although Co and Ag do not clearly de-mix for $x < 50$ in the solid state, they do not form a solid solution. If one considers that the configuration energy of an ideal solution is

$$E_c^{id} = \frac{1}{N}[xE_c(\mathrm{Co}) + NE_c(\mathrm{Ag})] \tag{5}$$

the 0 K excess energy of the system may be written as

$$\Delta E_c = E_c - E_c^{id} \tag{6}$$

where E_c is the configuration energy of the cluster. This excess energy was computed for the configurations predicted by Monte Carlo on the one hand and for configurations with the Co clustered at the centre on the other. The results are shown in Figure 4 where the excess energy is systematically found positive in both case. For $x < 30$, the predicted excess energies are lower than for Co at the centre because sub-surface positions are preferred. For $x > 50$, they are lower because the predicted Co groups at the centre form facets minimising this way the interfacial energy. For $x = 30$, which is the transition stoichiometry between Co beneath the surface and grouped at the centre, no significant prediction is obtained by Monte Carlo as two types of configurations are found equally probable. At these intermediate stoechiometries, temperature has no strong influence on Co grouping.

4 Conclusion

The predictions in this study can be summarised as follows. The configuration of Co_xAg_{201-x} clusters is mainly governed by two factors. One is the cluster morphology, which is typical to the nano-size, and the second is a balance between Co binding and Ag excess relaxation energy induced by cobalt. This is consistent with the previous experimental and model results like the burying of Co clusters in Cu [8,32] interpreted in term of capillarity. The two factors are found to compete and the cluster configuration to result from this competition. As a consequence, and depending upon the stoichiometry, the cluster centre may be a forbidden area for cobalt which then collects under vortices as isolated atoms or under {100}-facets in small groups preferentially forming pyramids. At elevated temperatures, higher than the melting temperature of the present clusters, like in bulk silver, these groups are predicted to dissolve but Co atoms are then distributed just below the surface. When the amount of Co is large enough, it regroups into a single group covered by silver and this group is stable at all temperatures investigated. Temperature however deteriorates the Ag coverage. When the central Co group is large enough to intersect the cluster surface, it preferentially takes part in {111}-facets. When Co is in majority, minimal free energy configurations correspond to Ag primarily occupying vortices and edges sites, as well as surface sites when their number is larger. The overall effect of temperature is to increase the importance of the Co binding relatively to the Ag relaxation, allowing for the formation of bigger groups of Co. Dissolution is only possible for low Co content and in the liquid phase. Since the Co–Co binding energy is larger than the Co–Ag binding energy, once the Co content is large enough, it precipitates at the centre of the cluster. Such characteristics are specific to non-miscible systems. Miscible systems form phases or solid solutions that consist, at thermodynamic equilibrium, in a uniform distribution in the core of the cluster surrounded by a shell where segregation may take place. This was found by MMC for Ni–Al and Cu–Au systems [9], and the trend toward such uniform distributions were also found by long two-dimensional molecular

dynamics simulations [4]. It however clearly appears that, although they form no solid solutions, small Co–Ag clusters only de-mix when the Co content is high.

The fact that, in nanoclusters, Co and Ag mix in stoechiometry and temperature dependent configurations is an important issue. It indicates indeed the possibility to monitor configurations by monitoring the stoechiometry and the temperature, which is experimentally feasible. The synthesis of controlled macroscopic Co–Ag mixed systems by such cluster assembling should thus be possible, provided assembling does not destroy the thermodynamically stable free cluster configurations identified in the present work.

This work was achieved in correspondence with the IAP5-1 research project promoted by the Belgian Federal Government.

References

1. J.L. Rousset, J.C. Bertolini, P. Miegge, Phys. Rev. B **53**, 4947 (1996)
2. J.M. Campillo, S. Ramos de Dibiaggi, A. Caro, J. Mater. Res. **14**, 2849 (1999)
3. E.E. Zhurkin, M. Hou, J. Phys. C **12**, 6735 (2000)
4. T.R. Kobayashi, K.S. Ikeda, Y. Shimizu, S. Sawada, Phys. Rev. B **66**, 245412 (2002)
5. F. Baletto, C. Mottet, R. Ferrando, Phys. Rev. Lett. **90**, 135504 (2003)
6. B. Degroote, A. Vantomme, H. Pattyn, K. Vanormelingen, M. Hou, Phys. Rev. B **65**, 195402 (2002)
7. B. Degroote, A. Vantomme, H. Pattyn, K. Vanormelingen, Phys. Rev. B **65**, 195401 (2002)
8. C.G. Zimmermann, M. Yeadon, K. Nordlund, J.M. Gibson, R.S. Averback, U. Herr, K. Samwer, Phys. Rev. Lett. **83**, 1163 (1999)
9. M. Hou, M. El Azzaoui, H. Pattyn, J. Verheyden, G. Koops, G. Zhang, Phys. Rev. B **62**, 5117 (2000)
10. G.E. Thayer, V. Ozolins, A.K. Schmid, N.C. Bartelt, M. Asta, J.J. Hoyt, S. Chiang, R.Q. Hwang, Phys. Rev. Lett. **86**, 660 (2001)
11. V. Ozolins, M. Asta, J.J. Hoyt, Phys. Rev. Lett. **88**, 096101 (2002)
12. G.E. Thayer, N.C. Bartelt, V. Ozolins, A.K. Schmid, R.Q. Hwang, Phys. Rev. Lett. **89**, 036101 (2002)
13. V. Dupuis, J. Tuaillon, B. Prével, A. Perez, P. Mélinon, G. Guiraud, F. Parent, L.B. Steren, R. Morel, A. Barthelemy, A. Fert, S. Mangin, L. Thomas, W. Wrensdorfer, B. Barbara, J. Magn. Mater. **165**, 42 (1997)
14. F. Parent, J. Tuaillon, L.B. Stern, V. Dupuis, B. Prével, A. Perez, P. Mélinon, G. Guiraud, R. Morel, A. Barthelemy, A. Fert, Phys. Rev. B **55**, 3683 (1997)
15. Yu.G. Pogorelov, G.N. Kakazei, J.B. Sousa, A.F. Kravets, N.A. Lesnik, M.M. Pereira de Azevedo, M. Malinowska, P. Panissod, Phys. Rev. B **60**, 12200 (1999)
16. J. Vergara, V. Madurga, J. Non-Cristal. Sol. **287**, 385 (2001)
17. V.G. Kravets, D. Bozec, J.A.D. Matthew, S.M. Thompson, H. Menard, A.B. Horn, A.F. Kravets, Phys. Rev. B **65**, 054415 (2002)
18. W. Bouwen, P. Thoen, F. Vanhoutte, S. Bouckaert, F. Despa, H. Weidele, R.E. Silverans, P. Lievens, Rev. Sci. Instrum. **71**, 54 (2000)
19. J.L. Rousset, F.J. Cadete Santos Aires, B.R. Sekhar, P. Mélinon, B. Prével, M. Pellarin, J. Phys. Chem. B **104**, 5430 (2000)
20. T.P. Martin, Phys. Rep. **273**, 199 (1996)
21. B. Pauwels, G. van Tendeloo, E. Zhurkin, M. Hou, G. Verschoren, L. Theil Kuhn, P. Lievens. Phys. Rev. B **63**, 165406 (2001)
22. S.M. Foiles, Phys. Rev. B **32**, 7685 (1985)
23. M.S. Daw, M.I. Baskes, Phys. Rev. B **29**, 6443 (1984)
24. J.H. Rose, J.R. Smith, F. Guinea, J. Ferrante, Phys. Rev. B **29**, 2963 (1984)
25. R.A. Johnson, Phys. Rev. B **41**, 9717 (1990)
26. R.A. Johnson, Phys. Rev. B **39**, 12554 (1989)
27. N.A. Levanov, V.S. Stepanyuk, W. Hergert, D.I. Bazhanov, P.H. Dederichs, A. Katsnelson, C. Massobrio, Phys. Rev. B **61**, 2230 (2000)
28. V.S. Stepanyuk, D.I. Bazhanov, W. Hergert, Phys. Rev. B **62**, 4257 (2000)
29. J.R. Regnard, J. Juanhuix, C. Brizard, B. Dieny, B. Mevel, Solid State Commun. **97**, 419 (1996)
30. T. Van Hoof, M. Hou, Appl. Surf. Sci. (in press)
31. M. Hou, V. Kharlamov, E.E. Zhurkin. Phys. Rev. B **66**, 195408 (2002)
32. V.S. Stepanyuk, D.V. Tsivline, D.I. Bazhanov, W. Hergert, A.A. Katsnelson, Phys. Rev. B **63**, 235406 (2001)